ResearchGate

See discussions, stats, and author profiles for this publication at: https://www.researchgate.net/publication/353543063

Monocoque Multirotor Airframe Design with Rotor Orientations Optimized for Direct 6-DoF UAV Flight Control

Conference Paper · August 2021

DOI: 10.2514/6.2021-2431

CITATIONS
0

READS
44

5 authors, including:

James Strawson
University of California, San Diego
11 PUBLICATIONS **97** CITATIONS
SEE PROFILE

Pengcheng Cao
University of California, San Diego
3 PUBLICATIONS **3** CITATIONS
SEE PROFILE

Falko Kuester
University of California, San Diego
184 PUBLICATIONS **2,097** CITATIONS
SEE PROFILE

Some of the authors of this publication are also working on these related projects:

Technical education in in a visualization environment View project

Simulations View project

All content following this page was uploaded by Pengcheng Cao on 03 August 2021.

The user has requested enhancement of the downloaded file.

Monocoque Multirotor Airframe Design with Rotor Orientations Optimized for Direct 6-DoF UAV Flight Control

James Strawson*, Pengcheng Cao †, Danny Tran‡, Thomas Bewley §, and Falko Kuester¶
University of California San Diego, La Jolla, CA 92093, USA

The search and rescue purposes of many VTOL UAVs are needed but there has been hardly new non-control research efforts recently improving the UAVs' flight agility and ability to survive in those hostile post-disaster environment. This paper introduces the design and analysis of a class of multirotor airframes with the capability of in-plane maneuverability and direct decoupled 6-DoF control which allow for low profile sensor payload integration without the need for a gimbal as well as predictable and safe flight in confined spaces such as tunnels and collapsed buildings. The case study of a hexrotor airframe is presented with its layout optimized via the methodology from the authors' previous work. The actuator combinations are tested and selected based on the performance metrics defined by authors, and utilized to restart the layout optimization. The aerodynamic performance of the platform is evaluated in several closed-quarter flight scenarios using CFD and compared with that of other airframe configurations. The structure of the single hollow monocoque shell is proposed and validated to obtain the desired shell thickness for the monocoque frame based on modal analyses and finite element methods. Finally, the flight controller developed by the authors is implemented and initial flight tests are conducted to validate the full actuation and a few more flight tests are to be done in the near future.

I. Introduction

Small UAVs with vertical take-off and landing (VTOL) capabilities are particularly suited for search and rescue efforts, allowing for easy field deployment, while providing a means to capture the context and content needed for situational awareness. These multirotor UAVs commonly use a quad, hex or octo-rotor design, requiring pitch and roll motion to maneuver in six-degree-of-freedom (6-DoF) space [1]. In disaster and post-disaster environments, where the UAV might have to hover close to a structure, transition into small openings, traverse corridors, while operating close to floors, walls, ceilings or other hard surfaces, maneuverability is a major concern [2]. Among the challenges are that (1) pitching and rolling requires additional space around the UAV to allow freedom of motion, (2) an articulated gimbal is necessary to keep the sensor payload level during flight which adds physical bulk to the UAV while increasing power consumption, and (3) maneuverability and predictability is severely reduced due to self-induced turbulence and prop wash [3].

Therefore, the UAV designs aiming at search and rescure purposes requires the following features to serve in the irregularly shaped spaces of post-disaster urban environment: (1) reduced flight footprint to realize agility, (2) ability to stabilize the sensor payload against turbulence and noises, (3) ability to avoid colliding with most of the obstacles, and if collision is unavoidable in some cases, the UAV is equipped with protective mechanisms increasing its structural resilience. In this paper, we propose the design of a monocoque hexrotor airframe assembled onto a hexrotor UAV with full actuation in 6 DoFs. This ducted, hollow monocoque is light weighted while provide structural resilience upon collisions. And its optimized rotor orientations grant it great maneuverability in 6-DoF flight.

This paper outlines phase two and three (see Fig. 1) of the illustrated development and validation procedure of a fixed-tilt multirotor UAV design[4] aiming to realize full actuation in all 6 DoFs, reduce the overall flight footprint of the UAV, and achieve high agility in turbulent environments[5]. The second phase design workflow is comprised of (1) component layout in conjunction with utility-driven design choices, (2) motor & propeller characterization, (3) aerodynamic performance simulation and analysis , and (4) monocoque airframe stiffness & modal analysis. The

*Robotics Engineer, ModalAI, Inc.
†Ph.D. student, Department of Mechanical and Aerospace Engineering.
‡Undergraduate student, Department of Mechanical and Aerospace Engineering.
§Professor, Department of Mechanical and Aerospace Engineering.
¶Professor, Department of Structural Engineering.

additive manufacturing (AM) technology is used for rapid prototyping of the proposed monocoque airframe. And the third phase readies the multirotor UAV with both hardware assembly and software implementation of decoupling flight controllers, and attempts to validate the system in the scenarios similar to those in the aerodynamic performance simulation. This paper presents an embodiment of the optimized layout rendered in authors' previous work [3, 6] through aforementioned workflow sub-steps as in phase 2 over 3 design iterations, and the experimental validation of full actuation and aerodynamic performance in the flight tests as in phase 3.

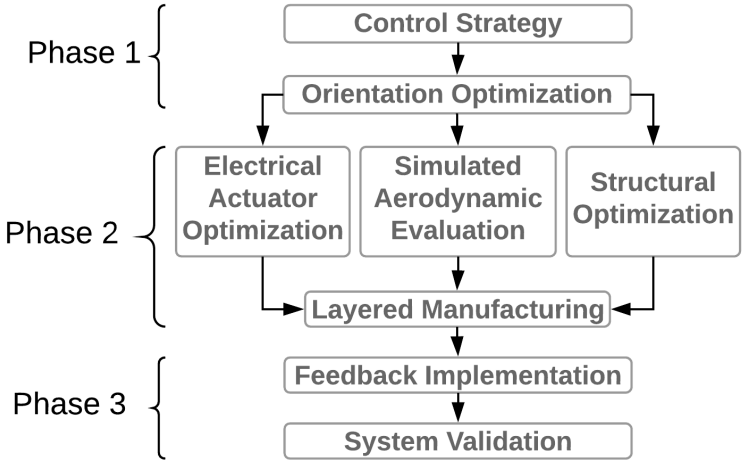

Figure 1 The design phases of a multirotor UAV with its airframe optimized for desired actuation authority.

II. Conceptual Design

The primary design goal is to create a small and configurable sensor platform for agile flight in confined spaces such as caves, tunnels, and collapsed buildings. However, the design must be parametric to allow scaling for significantly larger or smaller lift capacities. It must also allow rapid adaptation for new sensors and electronics payloads.

The vast majority of commercial multirotor designs use a central hub with radial arms supporting each motor, even in the case where the propellers are ducted or shrouded [7]. The authors propose, instead, a ducted multirotor where the ducting itself forms the primary load-bearing structure. This requires careful material selection and modal analysis to be viable, but results in a highly performant and elegant design with very low part count. The resulting protective ductwork is extremely resilient to impacts resulting from its material selection and it being the primary structural component as opposed to an afterthought in the design.

In this section, we introduce the general concept behind the monocoque airframe design. In Section II.A, we discuss how the rotor orientations of the hexrotor are optimized and how the other parameters of the airframe layout are determined. In Section II.B, we introduce the monocoque design and materials selected for manufacturing the airframe and discuss the reasons behind these approaches. And in Section II.C, we discuss the placement of mocap markers used to define the geometry needed in our motion caption system.

A. Rotor Orientations and Airframe Layout

When deciding the general configuration of the UAV platform, the authors select the hexrotor with tilted rotor orientations in light of both rotor redundancy and 6 degree-of-freedom (DoF) maneuverability [8]. The so-called "fixed-tilt" hexrotors, with an optimized airframe, can fully actuate its 6 DoFs while retaining the actuation and construction simplicity [9][10].

In authors' previous work, a multi-objective optimization (MOO) algorithm was developed to calculate the rotor orientations minimizing the objective function consists of the weighed minimum and maximum wrench in all 6 DoFs [11]. In a case study carried out in [11], we choose the maximum thrust force and drag torque of each motor to be $T_{max} = 4.72$ and $\tau_{d,max} = 0.0775Nm$, respectively. Before running the optimization, the airframe diameter of 0.45m and propeller diameter of 0.127m (5 inches) are pre-selected and are later found to converge greatly to the initial guesses. The take-off weight is selected to be $m_f = 0.700kg$ with the center of gravity estimated to be $0.023m$ below the airframe

geometric center because of the sensor payload, and each rotor arm (distance between airframe geometric center and each rotor's center of mass) is of the length $L_{arm} = 0.207m$. The resulting rotor orientations of this case study are as in (1), with an illustration of the optimized hexrotor airframe layout shown in Fig. 2. This result will serve as a basis of our airframe design in this paper.

$$
\begin{aligned}
V_1 &= [-0.173, 0.233, -0.957]^T, \\
V_2 &= [0.391, 0.031, -0.920]^T, \\
V_3 &= [-0.218, -0.195, -0.957]^T, \\
V_4 &= [-0.218, 0.195, -0.957]^T, \\
V_5 &= [0.391, -0.031, -0.920]^T, \\
V_6 &= [-0.173, -0.233, -0.957]^T.
\end{aligned} \tag{1}
$$

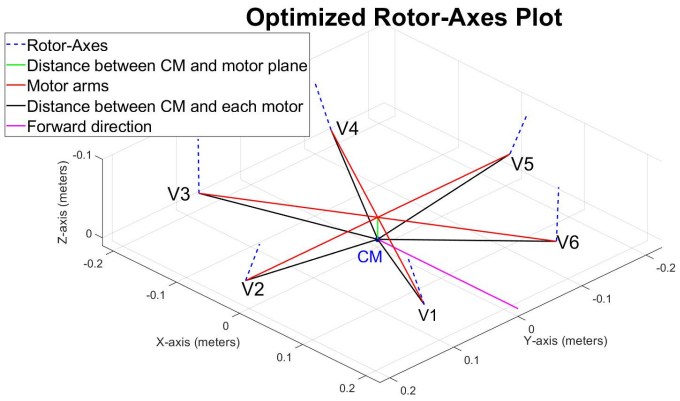

Figure 2 Optimized hexrotor layout with fixed-tilt rotor-axes in its body frame. The origin of the body frame is located at the center of mass(CM), and XYZ axes of the body frame conform to NED convention[12].

(a) **(b)** **(c)**

Figure 3 Hexrotor assembly with the monocoque airframe with frame diameter of 0.45m and propellers diameter 0.127m (5 inchs).

B. Monocoque Approach and Material Selection

The monocoque airframe is a hollow nylon shell that forms the shape of six propeller ducts in a hexagonal arrangement as shown in the final design in Fig. 3. In addition to supporting the motors, the shell acts as an impact-resilient crash structure to protect the payload and allow for collisions during flight in confined environments.

It is constructed on a large-format fused deposition modeling (FDM) printer [13] out of Taulman Nylon 910 due to its fantastic impact resiliency [14] and safety when printing indoors [15]. 3D printing the monocoque shell allows a completely hollow structure while still being a single piece. With injection molding, this construction would require at

least two separate parts and roto-molding would require a prohibitively complex arrangement of molds for this particular shape. Most importantly, additive manufacturing allows for very complex curved surfaces which is necessary due to the to arrangement of rotor angles optimally for 6DOF fight.

The shell can be seen in various prototype forms in Fig. 3c. These are all constructed on a 3DP-X1000 series FDM printer by 3D Platform which was chosen for its ability to print up to 1m x 1m x 50cm parts at equivalent resolutions to desktop 3D printers [13].

C. Motion Capture Marker Placement

A simple and scalable design feature that remained incorporated into the monocoque shell is the inclusion of mounting points for retroreflextive markers as visible in Fig.3. These markers are necessary for tracking the position and orientation of the airframe in a motion capture system for tuning and development of the flight controller. In the interest of allowing multiple unique platforms to fly simultaneously in a motion capture system for swarm research, the frame was designed with six irregularly positioned marker mounting positions such that any 3 markers define a unique geometry that can be identified by the motion capture software [16][17].

$$p = \frac{n!}{n_1!n_2!} = \frac{n!}{m!(n-m)!} \tag{2}$$

The theorem of permutations with repetition provides the means to calculate the number of possible marker arrangements on the same frame. For n total possible objects with n_1 identical objects of type 1 and n_2 identical objects of type 2, this theorem simplifies to the first expression of (2). This can be simplified to state that the number of permutations p of n objects with n_1 identical objects of type 1 and n_2 identical objects of type 2 is given by equ.2. Letting n be the number of mounting locations, m be the number of markers, and types 1 & 2 be the presence or absence of a marker in a specific mounting location, the number of possible unique permutations is given by the second expression of (2).

The minimum requirement of three markers for the motion capture system allows 20 permutations. However, using four markers allows for more robust object detection and still allows up to 15 multirotors to be uniquely identified, in addition to the six possible arrangements using five markers and the single case where all six locations are populated[16].

III. Actuators Characterization

The motors and propellers used in a multirotor are perhaps the most critical components to ensuring efficient and reliable flight. This testing sought to find the optimal combination of commercially available components suited for this airframe. The overall desired size of the airframe restricts the maximum propeller diameter to the common and widely-available five-inch standard, from which eight different propellers and twelve suitably-sized brushless motors were selected for testing.

A. Experiment

Each motor and propeller combination was attached to an RC Benchmark 1520 propeller thrust stand [18] affixed with a duct and motor mount mimicking those of the final monocoque frame pictured in Fig.4a. Each combination was then spun up to ten different throttle positions equally spaced between zero and 100% throttle where five samples were taken of current draw, rotational speed, and thrust over two seconds before being averaged and recorded. This process is fully automated for consistency.

The data collection process was repeated at both 7.4v and 11.1v mimicking the nominal voltage for both two and three-cell Lithium Polymer battery packs. This resulted in 192 individual test runs. For safety, the motors are powered by a current-limiting 10A power supply and several experiments reached this current limit, protecting the motor controller and preventing motor overheating and potential short circuits.

B. Results

Complete results, efficiency plots, and raw experiment data for every test conducted are available at `https://github.com/StrawsonDesign/motor_propeller_testing`.

An early estimate of the payload and overall airframe mass suggests that 1.47N thrust per motor would be required to hover, therefore efficiency in W/N at this thrust level formed the primary objective when choosing the motor and propeller combination. Many combinations result in excessive noise, vibration, and overheating and were flagged a

Table 1 Motors and Propellers Tested

Motors	Propellers
EMAX RS2205S 2600kv	Cyclone T5040C 3blade
Lumenier 1806-13 2500kv	Cyclone T5045C 3blade
Lumenier MX2206-9 2450kv	Gemfan 5x4.5 3blade
Lumenier RX2204-14 2300kv	Gemfan 5x4 2blade
Lumenier RX2205-12 2400kv	HQProp 5x4 4blade
Lumenier RX2206-11 2350kv	Lumenier 5x4.5 2blade
Lumenier RX2206-13 2000kv	Lumenier 5x4 3blade
Tiger Motor 1804-20 2400kv	Lumenier 5x5.3 3blade
Tiger Motor F40 III 2400kv	
Tiger Motor F40 Pro 2400kv	
Tiger Motor F30 2800kv	
Tiger Motor F30 2300kv	

non-viable during testing. These behaviors tend to produce poor numeric performance and flagged combinations did not appear high on a list sorted by efficiency.

Fig. 4b presents the efficiency curves for the top five most efficient combinations at 1.47N of thrust as calculated by interpolating between the two nearest samples during the experiment.

For this particular test and objective, the Lumenier RX2206-13 2000kv motor proved most efficient at both voltages when combined with a Lumenier 5x5.3 3-blade propeller at 7.4V and a Lumenier 5x4.5 2-blade propeller at 11.1V. While the most efficient combination for the 7.4V test was 3.6% more efficient the ideal combination of the 11.1V test, the two-blade propeller was chosen for the prototype build as the 7.4V testing was severely limited in maximum thrust and would impinge on the final system's controllability.

IV. Aerodynamic Simulation

Intentionally flying a toy quadcopter extremely close to a wall will usually result in it being drawn toward the wall due to Bernoulli's principle causing reduced pressure near the wall [19][20][21][22]. In this case, we hypothesize and verify that a side product of the fixed-tilt hexrotor airframe would be a small stabilizing effect causing the airframe to tend away from vertical surfaces without requiring control input.

A. Testing Scenarios and Parameters

Five near-object flight scenarios and an open-air baseline scenario are simulated using ANSYS Fluent to predict the change in forces acting on the airframe in a variety of plausible conditions. All simulations are configured to use incompressible air at $1atm$ and $300K$. The far-field boundary of all fluid domains are located (where applicable) a distance of 25 duct radii away from the airframe in all directions except downwards in which a distance of 50 duct radii was chosen, slightly larger than [23] since computational time was less of a concern. In all simulations, the hexacopter is treated as a rigid body with fixed orientation and flow is evaluated at steady-state. The design parameters are validated based on their performance in these simulations.

The simulated flight conditions apply to the airframe are as follows, and the preliminary results visualizing the streamlines of the air flow are shown in Fig. 5.

- Flight in open air
- 6cm above ground
- 6cm below a ceiling
- 6cm between nose and wall
- 6cm between right edge and wall
- Centered in a 1m x 1m x 6m tunnel

Each disk is modeled as an infinitely thin porous disk with the same swept area as the chosen Lumenier 5x4.5

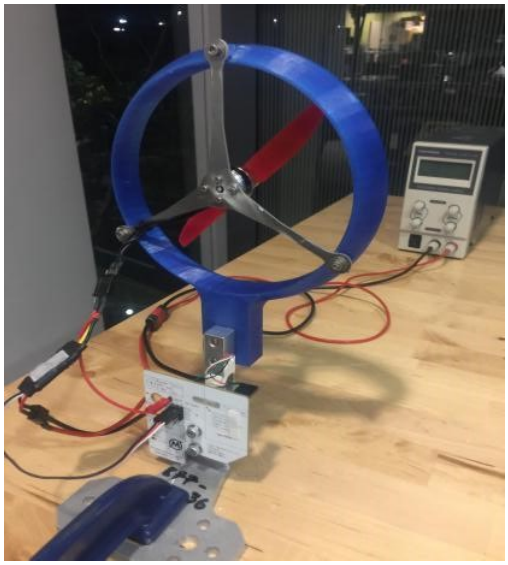

(a) Propeller test stand used for performance evaluation

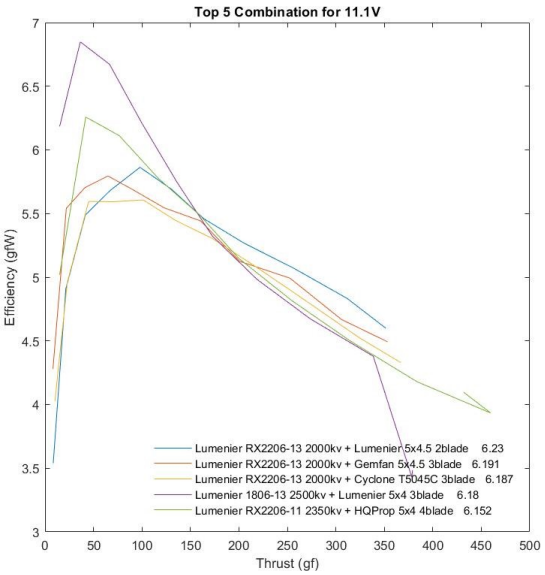

(b) Efficiency curves of 5 most efficient motor and propeller combinations at 11.1V

Figure 4 Propeller test stand and results

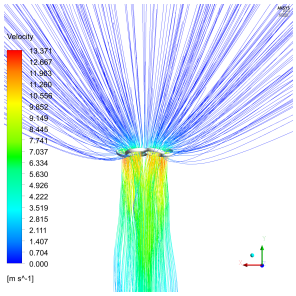

(a) Open Air

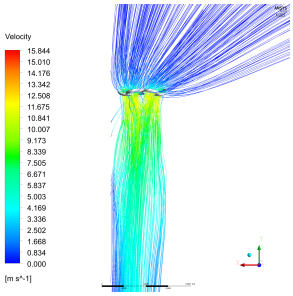

(b) Right Side 6cm From Wall

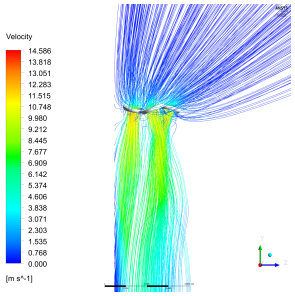

(c) Nose 6cm From Wall

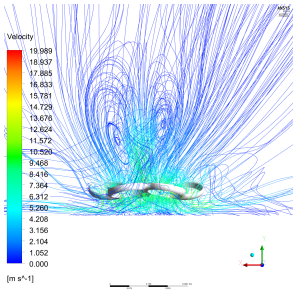

(d) 6cm Above Ground

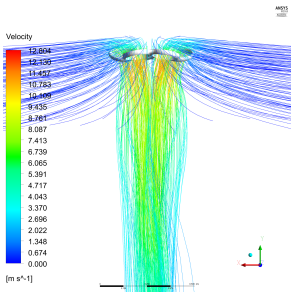

(e) 6cm Below Ceiling

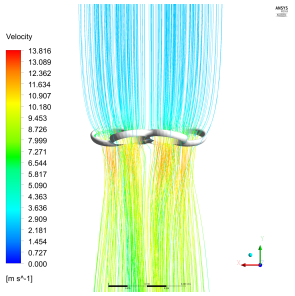

(f) Centered in 1m x 1m x 6m Tunnel

Figure 5 Streamlines plots for each CFD test scenario.

propeller. A uniform axial velocity distribution of incompressible air over the disk is assumed in accordance with actuator disk theory[24].

The fluid domain for each test case is created by performing boolean subtraction operation using the hexacopter's airfame and propeller hubs as tool bodies and an enclosing box as the target body. The topology of the box and actuator disks are merged to ensure the generation of a conforming mesh for continuous air flow. All fluid domains are

discretized into unstructured tetrahedrons and the actuator disks are meshed using a structured quadrilateral polar array configuration.

A region enclosing 5cm above, 60cm below, and 17cm around the airframe is meshed with five-times higher density than extremities of the domain to better capture the steeper gradients near the airframe and walls. The element count for the test cases ranged between 2.4 to 3 million.

The Reynolds-Averaged Navier-Stokes (RANS) turbulence model and Shear Stress Transport (SST) k-ω, are chosen to assess the aerodynamics forces exerted on the hexacopter. The PREssure STaggering Option (PRESTO) pressure interpolation scheme and Monotone Upstream-Centered Schemes for Conservation Laws (MUSCL) interpolation methods are used with the Semi-Implicit Method for Pressure-Linked Equations (SIMPLE) algorithm to resolve all simulations.

Table 2 Force components in Newtons. X axis points right (starboard), Y axis points upwards, and Z axis points rearwards.

Test Cases	$\mathbf{F_x}$	$\mathbf{F_y}$	$\mathbf{F_z}$
Open Air	0.013	7.073	0.113
Right Side 6cm From Wall	-0.206	6.547	0.658
Nose 6cm From Wall	-0.005	7.100	0.101
6cm Above Ground	-0.168	6.668	0.178
6cm Below Ceiling	-0.014	6.258	0.071
Centered in $1m$x$1m$x$6m$ Tunnel	0.020	7.425	0.013

B. Results and Qualitative Analysis

Table 2 presents the net forces experienced by the airframe when a fixed airflow required to support a $700g$ takeoff mass is applied to the actuator disks. Note that the frame is symmetric left-to-right but intentionally asymmetric forward-to-aft since the rotor angles are calculated with the methods presented in [11]. This predictably results in a near-zero force in the right-facing X axis for the open-air baseline case, for which the fluid flow can be seen in Fig. 5a.

In the scenario where the airframe's right side is against a wall, a beneficial additional stabilizing force of $0.2N$ away from the wall is predicted by the model. This partly confirms the hypothesis for this scenario, the streamlines for which are depicted in Fig. 5b. The simulation scenario with the airframe's nose against a wall does provide $0.1N$ stabilizing force away from the wall, however this is roughly the same forced experienced in the open-air baseline. As such, any trimming of the airframe attitude by the feedback controller would negate this. Note that this near-zero change in force is still vastly favorable to being pulled towards the wall.

When the airframe is $6cm$ above ground, as depicted in Fig. 5d, there is significant air recirculation and irregular flow due to in ground effect (IGE) causing a decrease in lift. Hovering this close to the ground is extremely unstable as explored in [21] and [22] and provides additional justification for the higher frequency response afforded by the fully actuated 6-DoF control scheme as presented in [11].

V. Structural Characterization

The overall shape of the hollow monocoque frame is determined by the duct size and profile. This leaves the thickness of the shell to be determined through careful structural modeling. Due to the overall design, the loading on the motor mounts and frame are minimal. Instead, potential interaction of the feedback controller with vibrational modes of the structure are of primary concern. The design goals include a feedback controller with a crossover frequency between 8Hz and 10Hz, it is therefore desirable to have the primary vibrational modes at least one order of magnitude faster to avoid interaction.

A. Finite Element Model and Boundary Conditions

To facilitate rapid adjustment and computational solution of the model, an initial CAD model of the monocoque shell was drawn entirely of surfaces to facilitate modeling with S4R shell elements. The finite element (FE) model can then be adjusted for thickness very easily without changing the CAD model. To mimic the attachment of a heavy and rigid payload module, all 6 mounting points on the inner surface of the shell are fixed in place. Finally, six point-masses of

30g each are added to the motor mounting locations on the frame to replicate the effects of the motors on the vibrational modes of the frame. The FE model was given a homogeneous modulus of elasticity as $72,932PSI$ as provided by the material manufacturer's specification [14].

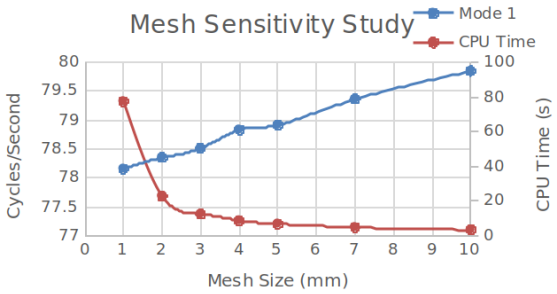

Figure 6 Results of mesh sensitivity study

A mesh sensitivity analysis is performed over several element sizes to confirm that the resulting natural frequencies are feasible in a finite element environment and to determine a mesh size that balances accuracy with compute time. The study evaluates mesh sizes ranging from 10mm to 1mm and the authors concluded that a mesh size of 3mm formulates a suitably converged result with a reasonable compute time of 12.6 seconds to solve the model.

B. Results and Validation

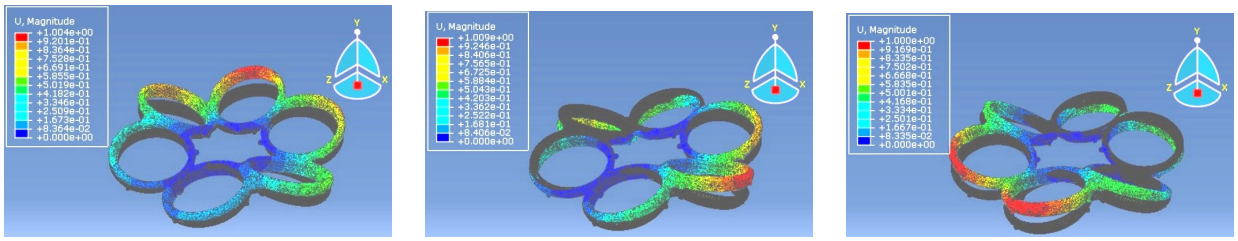

(a) Mode 1 82.1Hz **(b)** Mode 2 83.4Hz **(c)** Mode 3 97.6Hz

Figure 7 Displacement plots of first 3 vibrational modes of the finite element shell model

Since the 3DP printer chosen to manufacture the frame has extrusion nozzle sizes of 0.25, 0.4, 0.6, and 0.8mm available, these are chosen as the shell thicknesses for analysis[13]. The 0.4mm shell has its first three vibrational modes at frequencies of 82.1, 83.4, and 97.6Hz which are right at the design goal. Displacement plots indicating the directions of flex for these three modes are presented in Fig. 7.

To validate the solid model, we perform a static analysis of the stiffness in the direction of deformation when the shell is under its primary (slowest) vibrational mode. We support the mounting points of the shell rigidly then use a force gauge to deform the body with 6mm of deflection where the force gauge is applied. This required 11.5N of force which is only 3.5% from the 11.9N predicted force required to deform the FE model under static point load.

VI. Layered Manufacturing

After the modal analyses are performed, the authors have found the $0.4mm$ shell thickness with the material property of the nylon filament can keep the first 3 vibrational modes at frequencies slightly below 100 Hz. With only the $0.4mm$ thickness reaching our design goal, we decide to manufacture a prototype of the airframe of this shell thickness using the additive manufacturing techniques with the available lab facilities. A 3D Platform 1000 3D Printer [13] with a 0.4 mm nozzle was equipped with Taulman Nylon 910 filament [14] to manufacture our prototype as shown in Fig. 8. After fine-tuning the printer's settings, we ran 4 prints in a row smoothly without interruptions or failures. Each print consumed 53 hours 47 min on average, and all of them rendered a prototype of the airframe of acceptable quality. The authors also managed to shoot the timelapse video of one print which is can accessed here:

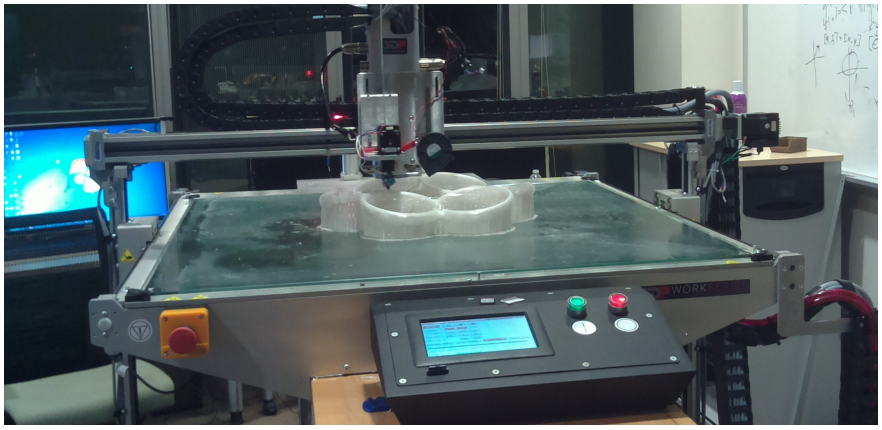

Figure 8 Manufacturing the airframe using the 3D Platform printer

https://www.youtube.com/watch?v=rdhvcgdSPiA. In the end, all the prototypes monocoque airframes have an average weight of 342 grams.

VII. Flight Control Implementation

Although beyond the requirements of Phase 2 tasks illustrated in Fig. 1, the author has already achieved preliminary real-world test flights with feedback control scheme at this point. As shown in Fig. 3b, the airframe is assembled with one LiPo battery, one flight controller board, one power distribution board, 6 electronic speed controllers (ESCs) and their corresponding motors and propellers. These hardware pieces are selected based on test results or empirical UAV design rules. After readying all the hardware, the flight control software is designed and implemented for both simulations and test flights.

A. Hardware Selections

As for the LiPo batttery, we choose Lumenier 1800mAh 3s 35c Lipo battery (11.1 V nominal voltage) for its compact size and sufficient capacity to power 6 motors to hover the hexrotor for more than 30 min when fully charged. And the flight controller board we use here is a BeagleBone Blue for its light weight and low expense, which is paired with a power distribution board to connect to 6 ESCs. In addition, our ESCs are selected as Lumenier Mini 20A ESCs with customized SimonK firmware for its light weight and steady current control to the motors. Last but not least, our motors and propellers are selected to be Lumenier RX2206-13 2000kv motors and Lumenier 5x4.5 2-blade propeller, respectively, according to the experimental results in Section III.B. The assembled UAV has a take-off weight of $704g$, which has acceptable errors compared to the parameter on which we run the optimization in Section II.A.

B. Flight Control Software

The mathematical modeling of the fixed-tilt hexrotor's flight dynamics has been presented in authors' previous work [25]. Based on the derived equations of motion, a flight controller has been developed, aiming to decouple the translational and rotational dynamics and to resist disturbance in narrow space scenarios. The flight controller is designed using the linear quadratic regulator (LQR) method, and aims to stabilize the error dynamics with noises and disturbances in all its 6 DoFs. The controller gains are inspected to ensure the crossover frequency to be between $8Hz$ and $10Hz$ in the simulations. The controller architecture is shown in Fig. 9 below. And a preliminary implementation of the flight controller can be watched on: https://www.youtube.com/watch?v=0P7kTeUToKM. One can notice that the flight controller well stabilizes the hexrotor's attitude, while it is difficult for the hexrotor to overcome drifts when commanded to move sideways. The future work will involve tests in the near-wall and close-to-ground scenarios similar to the simulation setups in Section IV in order to furthur validate our system.

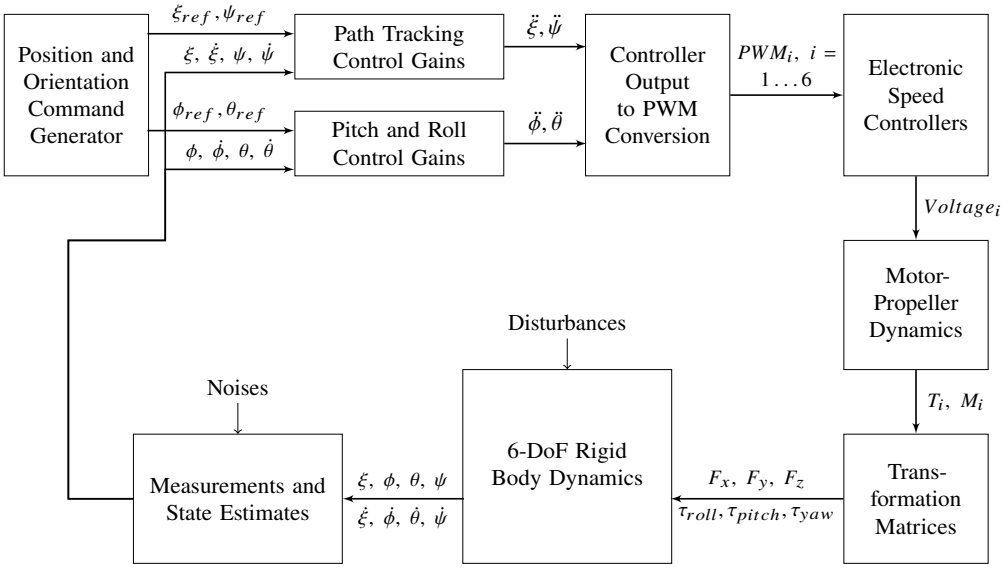

Figure 9 Fixed-tilt hexrotor control scheme architecture.

VIII. Conclusions

This paper demonstrates the overarching design, analyses, and validation of a shelled monocoque frame hexacopter focused on utilizing the rotor angle optimization method presented in [11]. The conceptual design stage renders a monocoque airframe of the fixed-tilt hexrotor layout. The effectiveness of the ducted monocoque airframe is validated in aerodynamic simulations in tending away from confined surfaces with no flight commands. And the actuators characterization manages to find an optimal combination of motor and propeller based on the efficiency metrics. In addition, the structural analysis suggests a 0.4mm shell thickness to help reach the vibrational design goal. And furthermore during the prototyping of the airframe, our 3D printing facility prints the airframe weighing $342g$ in around 54 hours. Last but not least, we assemble the hardware and support structures onto the airframe and performs test flights using our self-made software, thus validating the effectiveness of our airframe design.

The results show that highly complex surface bodies such as a monocoque frame lend themselves well to rapid design revisions utilizing shell finite element analysis and that this 3D printed structure performs similarly to its finite element stiffness model. In addition, the simulations also suggest that a tilted rotor layout can provide beneficial stabilizing fluid interactions in some confined flight scenarios.

Acknowledgement

This work was supported by the National Institute for Standards and Technology (NIST) under award #70NANB17H21, "Improving Disaster Resilience Through Scientific Data Collection with UAV Swarms," and the National Science Foundation (NSF) under award #DGE-0966375, "Training, Research and Education in Engineering for Cultural Heritage Diagnostics." Additional support was provided by the NSF under award #CNS-1338192, "MRI: Development of Advanced Visualization Instrumentation for the Collaborative Exploration of Big Data," as well as the Kinsella Heritage Engineering Fund and the Qualcomm Institute at UC San Diego. Opinions, findings, and conclusions from this study are those of the authors and do not necessarily reflect the opinions of the research sponsors. The authors would also like to thank a team of students from UC San Diego: He Huang, Yifan Xu, and Mingchen Mao for their help and inspiration on the selection and testing of motors and propellers.

References

1. Naidoo, Y., Stopforth, R. & Bright, G. Quad-Rotor unmanned aerial vehicle helicopter modelling & control. *International Journal of Advanced Robotic Systems* **8,** 45 (2011).
2. Adams, S. M. & Friedland, C. J. *A survey of unmanned aerial vehicle (UAV) usage for imagery collection in disaster research and management* in *9th international workshop on remote sensing for disaster response* **8** (2011).

3. Strawson, J. *Feedback Control Driven Mechanical Design Optimization.* PhD thesis (UC San Diego, 2018). https://escholarship.org/uc/item/8w82m5n8.

4. Rashad, R., Goerres, J., Aarts, R., Engelen, J. B. C. & Stramigioli, S. Fully Actuated Multirotor UAVs: A Literature Review. *IEEE Robotics Automation Magazine* **27,** 97–107 (2020).

5. Shimizu, T., Suzuki, S., Kawamura, T., Ueno, H. & Murakami, H. Proposal of 6DOF multi-copter and verification of its controllability. *Society of Instrument and Control Engineers of Japan (SICE), 2015 54th Annual Conference of the,* 810–815 (July 2015).

6. Strawson, J., Cao, P., Bewley, T. & Kuester, F. *Rotor Orientation Optimization for Direct 6 Degree of Freedom Control of Multirotors* in *IEEE Aerospace Conference* (2021).

7. Habsi, S. A., Shehada, M., Abdoon, M., Mashood, A. & Noura, H. *Integration of a Vicon camera system for indoor flight of a Parrot AR Drone* in *2015 10th International Symposium on Mechatronics and its Applications (ISMA)* (Dec. 2015), 1–6.

8. Rashad, R., Goerres, J., Aarts, R., Engelen, J. B. & Stramigioli, S. Fully actuated multirotor UAVs: A literature review. *IEEE Robotics & Automation Magazine* **27,** 97–107 (2020).

9. Rajappa, S., Ryll, M., Bülthoff, H. H. & Franchi, A. *Modeling, control and design optimization for a fully-actuated hexarotor aerial vehicle with tilted propellers* in *2015 IEEE international conference on robotics and automation (ICRA)* (2015), 4006–4013.

10. Jiang, G., Voyles, R., Sebesta, K. & Greiner, H. *Estimation and optimization of fully-actuated multirotor platform with nonparallel actuation mechanism* in *2017 IEEE/RSJ International Conference on Intelligent Robots and Systems (IROS)* (2017), 6843–6848.

11. Strawson, J., Cao, P., Bewley, T. & Kuester, F. *Rotor orientation optimization for direct 6 degree of freedom control of multirotors* in *2021 IEEE Aerospace Conference (50100)* (2021), 1–12.

12. Junkins, J. L. & Schaub, H. *Analytical mechanics of space systems* (American Institute of Aeronautics and Astronautics, 2009).

13. *Large Format 3D Printer for Industrial Additive Manufacturing* https://3dplatform.com/.

14. *Taulman 910 Nylon Polymer* http://taulman3d.com/alloy-910-spec.html.

15. Kriek, G., Lazear, N., Rhodes, V., Barnes, J., Bollmeier, J., Chuang, J. C., Holdren, M. W., Wisbith, A. S., Hayward, J. & Pietrzyk, D. Development of Emission Factors for Polyamide Processing. *Journal of the Air & Waste Management Association* **51,** 1001–1008. eprint: https://doi.org/10.1080/10473289.2001.10464329. https://doi.org/10.1080/10473289.2001.10464329 (2001).

16. Limited, V. M. S. *Vicon System Reference, Revision 1.4* http://bdml.stanford.edu/twiki/pub/Haptics/MotionDisplayKAUST/%20/ViconHardwareReference.pdf.

17. VICON. *Vicon DataStream SDK 1.7.0 Developer's Manual, Vicon Motion Systems Ltd. 2016* https://www.vicon.com/downloads/utilities-and-sdk/datastream-sdk.

18. *RC Benchmark Propeller Thrust Stand* https://www.rcbenchmark.com/dynamometer-series-1520/.

19. Powers, C., Mellinger, D., Kushleyev, A., Kothmann, B. & Kumar, V. *Influence of Aerodynamics and Proximity Effects in Quadrotor Flight* in *Experimental Robotics: The 13th International Symposium on Experimental Robotics* (eds Desai, J. P., Dudek, G., Khatib, O. & Kumar, V.) 289–302 (Springer International Publishing, Heidelberg, 2013). ISBN: 978-3-319-00065-7. https://doi.org/10.1007/978-3-319-00065-7%5C_21.

20. Robinson, D. C., Chung, H. & Ryan, K. Computational investigation of micro rotorcraft near-wall hovering aerodynamics. *2014 International Conference on Unmanned Aircraft Systems (ICUAS)* (2014).

21. Gourdain, N., Singh, D., Jardin, T. & Prothin, S. Analysis of the Turbulent Wake Generated by a Micro Air Vehicle Hovering near the Ground with a Lattice Boltzmann Method. *Journal of the American Helicopter Society* **62,** 1–12 (2017).

22. Ganesh, B., Komerath, N., Pulla, D. P. & Conlisk, A. *Unsteady aerodynamics of rotorcraft in ground effect* in *43rd AIAA Aerospace Sciences Meeting and Exhibit* (2005), 1407.

23. Yoon, S., Lee, H. C. & Pulliam, T. H. *Computational Analysis of Multi-Rotor Flows* in *54th AIAA Aerospace Sciences Meeting* (2016), 0812.

24. Keck, R.-E. A numerical investigation of nacelle anemometry for a HAWT using actuator disc and line models in CFX. *Renewable Energy* **48,** 72–84. ISSN: 0960-1481. http://www.sciencedirect.com/science/article/pii/S0960148112002455 (2012).

25. Cao, P., Strawson, J., Bewley, T. & Kuester, F. *Decoupled Translational and Rotational Flight Control Designs of Canted-Rotor Hexacopters* in *AIAA Scitech 2021 Forum* (2021), 1058.

View publication stats